LLNL-JRNL-857714

Lawrence Livermore National Laboratory

Direct mechanistic connection between acoustic signals and melt pool morphology during laser powder bed fusion

Y. Sun, S. Gorgannejad, A. Martin, J. Nicolino, M. Strantza, J.-B. Forien, V. Thampy, S. Liu, P. Quan, C. J. Tassone, M. J. Matthews, N. P. Calta

Applied Physics Letters

Disclaimer

Lawrence Livermore National Laboratory is operated by Lawrence Livermore National Security, LLC, for the U.S. Department of Energy, National Nuclear Security Administration under Contract DE-AC52-07NA27344.

AUTHOR QUERY FORM

AIP Publishing	Journal: Appl. Phys. Lett. Article Number: APL24-AR-01934	Please provide your responses and any corrections by annotating this PDF and uploading it to AIP's eProof website as detailed in the Welcome email.

Dear Author,

Below are the queries associated with your article; please answer all of these queries before sending the proof back to AIP.

Article checklist: In order to ensure greater accuracy, please check the following and make all necessary corrections before returning your proof.

1. Is the title of your article accurate and spelled correctly?
2. Please check affiliations including spelling, completeness, and correct linking to authors.
3. Did you remember to include acknowledgment of funding, if required, and is it accurate?

Location in article	Query / Remark: click on the Q link to navigate to the appropriate spot in the proof. There, insert your comments as a PDF annotation.
AQ1	Please check that the author names are in the proper order and spelled correctly. Also, please ensure that each author's given and surnames have been correctly identified (given names are highlighted in red and surnames appear in blue).
AQ2	Please define PCB and TMS at first occurrence.
AQ3	Please provide publisher's name for Refs. 14 and 30.
AQ4	Please provide thesis type for Ref. 31.
	Please confirm ORCIDs are accurate. If you wish to add an ORCID for any author that does not have one, you may do so now. For more information on ORCID, see https://orcid.org/.
	Yuchen Sun - 0000-0001-5994-8961 Sanam Gorgannejad - 0000-0002-4508-7256 Aiden Martin - 0000-0003-2362-5524 Jenny Nicolino- Maria Strantza- Jean-Baptiste Forien - 0000-0002-9229-2455 Vivek Thampy - 0000-0003-3983-3109 Sen Liu- Peiyu Quan - 0000-0003-3338-5106 Christopher J. Tassone- Manyalibo J. Matthews - 0000-0003-3519-7221 Nicholas P. Calta - 0000-0002-6327-6640

	Please check and confirm the Funder(s) and Grant Reference Number(s) provided with your submission: Basic Energy Sciences, Award/Contract Number DE-AC02-76SF00515 Lawrence Livermore National Laboratory, Award/Contract Number DE-AC52-07NA27344 Lawrence Livermore National Laboratory, Award/Contract Number 21-ERD-008 Please add any additional funding sources not stated above:

Thank you for your assistance.

Applied Physics Letters ARTICLE pubs.aip.org/aip/apl

Direct mechanistic connection between acoustic signals and melt pool morphology during laser powder bed fusion

Cite as: Appl. Phys. Lett. 125, 000000 (2024); doi: 10.1063/5.0205663
Submitted: 27 February 2024 · Accepted: 1 July 2024 ·
Published Online: 0 Month 0000

View Online Export Citation CrossMark

Yuchen Sun,[1,a)] Sanam Gorgannejad,[1] Aiden Martin,[1] Jenny Nicolino,[1] Maria Strantza,[1] Jean-Baptiste Forien,[1] Vivek Thampy,[2] Sen Liu,[2] Peiyu Quan,[2] Christopher J. Tassone,[2] Manyalibo J. Matthews,[1] and Nicholas P. Calta[1]

AFFILIATIONS

[1]Lawrence Livermore National Laboratory, Livermore, California 94550, USA
[2]SLAC National Accelerator Laboratory, Menlo Park, California 94025, USA

[a)]Author to whom correspondence should be addressed: sun38@llnl.gov

ABSTRACT

Various nondestructive diagnostic techniques have been proposed for in situ process monitoring of laser powder bed fusion (LPBF), including melt pool pyrometry, whole-layer optical imaging, acoustic emission, atomic emission spectroscopy, high speed melt pool imaging, and thermionic emission. Correlations between these in situ monitoring signals and defect formation have been demonstrated with acoustic signals having been shown to predict pore formation with especially high confidence in recent machine learning studies. In this work, time-resolved acoustic data are collected in both the conduction and keyhole welding regimes of LPBF-processed Ti-6Al-4V alloy. A non-dimensionalized Strouhal number analysis, used in whistle aeroacoustics, is applied to demonstrate that the acoustic signals recorded in the keyhole regimes can be directly associated with the vapor depression morphology. This mechanistic understanding developed from whistle aeroacoustics shows that acoustic monitoring during the LPBF process can provide a direct probe into the vapor depression dynamics and defect occurrence, especially in the keyhole regimes relevant to printing and defect formation.

Laser powder bed fusion (LPBF), previously called selective laser melting (SLM), is an additive manufacturing (AM) approach for metal components that has proven to be an exceptionally useful fabrication technique in many commercial and industrial applications.[1] LPBF AM provides various advantages compared to conventional manufacturing approaches, such as geometric flexibility, low production lead time, and inexpensive tooling. Alongside the increasing adoption of this additive manufacturing method, significant effort has also been made to control, predict, and understand the phenomena governing the process. While their overall behavior is predictable based on laser printing parameters,[2,3] specific defect formation events are often stochastic and unpredictable, especially when considering the varying thermal boundary conditions driven by the high degree of geometric flexibility that additive approaches permit and the tremendous number of competing physical properties of the material, including laser absorptivity, melting temperature, and thermal conductivity.[4–6] As a result, part qualification often requires extensive destructive testing in addition to inspection through computed tomography (CT). While reliable, this can be time consuming, financially costly, and not always well suited for the small defects and complex geometries associated with AM-printed parts. As such, in situ characterization techniques are well suited as a preliminary "failure" test criteria with remarkably low time and cost requirements.

Many different modalities have been proposed for in situ process monitoring during LPBF, including melt pool pyrometry,[7–9] whole-layer optical imaging,[10,11] acoustic emission,[12–16] high-speed melt pool imaging,[17,18] and thermionic emission.[19] A correlation between these in situ monitoring signals with defect formation has been demonstrated in various systems.[20–24] Furthermore, machine learning studies have shown qualitative correlation between acoustic signals and feature formation as it varies with print parameters.[25–31] Recent work with machine learning models has shown high probability for pore detection by combining photodiode with acoustic monitoring data in single-track prints.[32] Acoustic monitoring offers complementary information to optical methods and permits greater flexibility by not requiring optical line-of-sight to the build. However, broader adoption of

Applied Physics Letters ARTICLE pubs.aip.org/aip/apl

acoustic methods has suffered from a lack of mechanistic understanding compared to, for example, pyrometry where the physics of black-body radiation is well understood. In pursuit of strengthening confidence in acoustic monitoring, a more mechanistic understanding of acoustic signal generation in LPBF is necessary. This work aims to develop a mechanistic connection between the acoustic signal and melt pool behavior during LPBF through analysis of single-track prints using a whistle aeroacoustic model.

Acoustic signals were recorded during laser irradiation of 3 mm long single laser tracks on Ti-6Al-4V bare plate performed using a 1070 nm continuous wave Yb-fiber laser (YLR-500-AC-Y14, IPG Photonics) focused to a D4σ diameter of ~73 μm, laser scan speeds of 250 and 500 mm/s, and laser powers between 100 and 400 W. The experimental platform used in the present work has been described previously.[33] Laser direction and scan speed were controlled by a SCANLAB intelliSCAN scan head, which consists of a two-axis galvanometer scanning mirror system. A 1/4″ free-field, prepolarized microphone and preamplifier package (frequency range: 4–100 000 Hz (+2/−3 dB), dynamic range: 165 dB, 378C01, PCB Piezotronics, Inc.) was installed with direct line-of-sight to the laser-sample coincident plane at 44° offset angle and a working distance of 140 mm. In situ x-ray imaging was performed at SLAC National Accelerator Laboratory's Stanford Synchrotron Radiation Lightsource (SSRL) beamline 2-2 using white-beam x-ray spectrum transmission x-ray images of the LPBF process captured using a scintillator-based optical system,[32] operating at 20 kfps with an effective pixel size of 2 μm per pixel. The vacuum chamber containing the sample was evacuated to ~5 × 10^{-2} Torr prior to being filled with 730 Torr argon inert gas environment for processing. Argon was constantly flowed through the vacuum chamber during experiments using a high-efficiency air knife (Super Air Knife, Aluminum, 3 in., EXAIR) located above the substrate surface. During processing, the laser was scanned across a Ti-6Al-4V substrate (TMS Titanium, Poway, CA, USA) as a 2.5 mm long single line. Each substrate was approximately 500-μm thick in the x-ray probe direction.

The acoustic data are presented in the frequency domain in time-independent and time-dependent plots, generated by Fourier transforms and wavelet transforms, respectively (Fig. 1). Plots are shown for three prints performed with a scan speed of 500 mm/s and laser powers of 100, 200, and 400 W, corresponding to the conduction, stable keyhole, and unstable keyhole regimes, respectively. The conduction regime is comprised of scans throughout which the depth-to-width ratio of the vapor depression remains below 1, while for the keyhole regimes, the ratio is greater than 1. Prints where pores are identified are further classified under the unstable regime.

The 100 W case shows a narrow band of tone frequencies centered around 70 kHz, which is consistent with stable melt pool geometry observed in x-ray videos. Despite the consistency in frequency, fluctuations in the acoustic signal are observed with occasional short-lived peaks arising and fading. The stochasticity in acoustic signals notably increases with scan power, with tone frequency ranges of 40–60 kHz at 200 W and 30–80 kHz at 400 W. Distinctly, at 400 W, these ranges are not only constituted of narrowband peaks (~10 kHz wide) scattered across the wider range but also a handful of broadband peaks that span nearly the entire 30–80 kHz range. Interestingly, there are also cases where peaks are long-lived enough in time (>200 μs) to experience a shift in frequency between when they first appear and when they fade. Although this overall stochastic acoustic behavior is easily correlated with high normalized enthalpy, unstable keyhole morphology, and defect formation,[34–36] a deeper interpretation of the specific features we observe requires mechanistic understanding of the acoustic phenomena.

Interpretation of the acoustic signals first requires consideration of the various acoustic sources present in the LPBF process, including melt pool waves, solidification phenomena, and events deeper in the material. Examination of the signal magnitude prior to the start of the print shows that ambient experimental signals are negligible, including the Ar gas recirculation system, vacuum pumps, galvo motion, and other periphery systems. The low residual stress build-up in single-track Ti-6Al-4V prints makes solidification cracking rare. The acoustic impedance mismatch between solid Ti and gaseous Ar hinders subsurface acoustic signals reaching the airborne microphone; calculations suggest that <1% of acoustic energy generated within solid or liquid metal would be transmitted to a surrounding gas environment.[37,38] As such, the airborne microphone effectively couples to gas flow associated with the vapor depression and reduces signal from potential subsurface sources, like cracking and bubble collapse. We are confident the acoustic signals recorded and analyzed are metal vapor aeroacoustics directly coupled to the vapor depression. To interpret these metal-vapor aeroacoustics and extract some mechanistic insight into vapor depression dynamics, we analyze through the perspective of whistle aeroacoustics.

A classic and elegant example of the whistle model is the steam kettle whistle, which can be defined as a cylinder with two similarly sized holes axially aligned on opposing chamber faces [Fig. 2(a)]. The upstream hole connects the whistle body to a large chamber of higher pressure relative to ambient where the gas flow originates, and the downstream hole connects the whistle body with an ambient atmosphere; as gas flows through the whistle, a tone is generated. The specific mechanisms by which tones are generated can be classified into three classes[39] and—for a given system—may vary based on the Reynolds number $Re = Ud/\nu$, where U is the gas velocity, d is the opening diameter, and ν is kinematic viscosity.[40,41] Analysis of steam kettle whistles has shown that as the Reynolds number changes, there are two regimes of whistle behavior; these regimes can be identified by the Strouhal number $St = fd/U$, where f is the tone frequency, d is the opening diameter, and U is the gas velocity.[42] At low Reynolds number (i.e., low air velocity, large hole diameter), the emitted acoustic frequency is constant, corresponding to a Helmholtz resonator condition where the Helmholtz cavity is defined as the whistle cylinder and the effective neck length is the sum of the plate thicknesses. At high Reynolds number (i.e., high air velocity, small hole diameter), the Strouhal number is constant, corresponding to a class III whistle, which entails vortex shedding at the end of a resonating duct, similar to a flute or organ pipe.[41]

Figure 2(b) is a radiograph of a vapor depression resulting from a single-track print at 500 mm/s and 300 W. Contrast enhancement, binarization, and median filtering are performed on the radiograph to generate Fig. 2(c). We analogize the keyhole-regime vapor depression as a whistle such that the whistle body is the larger chamber of height h and diameter D, as shown in Fig. 2(d). The gas flow source associated with the upstream hole is the vapor jet with velocity U generated by evaporation near the incident point of the laser beam at the bottom of the vapor depression,[43] and the downstream hole would be the

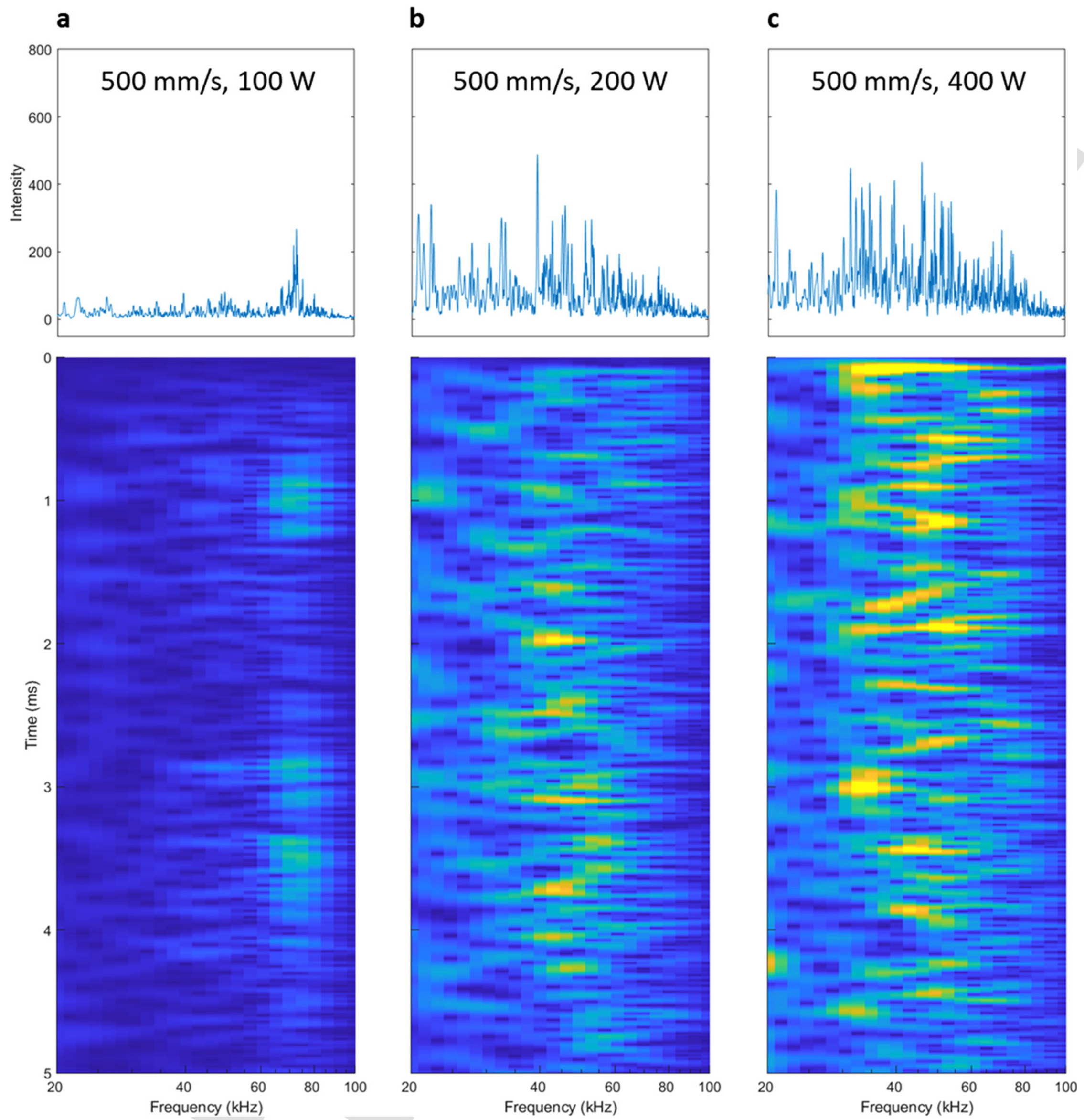

FIG. 1. Time-independent Fourier transforms (top) and time-dependent wavelet transforms (bottom) of acoustic data recorded during single-track irradiations on Ti-6Al-4V bare plate with laser scan speed 500 mm/s and laser powers of (a) 100, (b) 200, and (c) 400 W. These powers correspond to the conduction, stable keyhole, and unstable keyhole regimes of print behavior, respectively.

narrower neck of the vapor depression defined by diameter d. While not all depressions will fit this model, we hypothesize that the system will generate acoustic signal via a whistle mechanism when the vapor depression dynamics align with the whistle model—i.e., tones occur when gas flows through a larger chamber followed by a narrower opening.

We proceed to demonstrate that vapor depressions can exhibit whistle behavior through a non-dimensionalized analysis of the melt pool aeroacoustic behavior. Precise calculation of the Reynolds number requires kinematic viscosity of the flowing gas. This is difficult to estimate from literature values due to the mixing of gaseous metal with argon at the extreme temperatures present. However, the Reynolds number has been calculated using the density of the background gas and surface temperature at the location of the laser spot.[44] With constant background gas pressure and surface temperature in the laser spot increasing monotonically with laser power, the Reynolds number is expected to also increase monotonically with laser power. To permit incorporation of data from a wide range of experimental and material parameters, normalized enthalpy can be used in place of laser power.[45,46] Since our current scope focuses on changes in laser power at two scan speeds, we use a reduced form of normalized enthalpy $P/u^{1/2}$, with laser power P and scan speed u. From these relations,

Applied Physics Letters ARTICLE pubs.aip.org/aip/apl

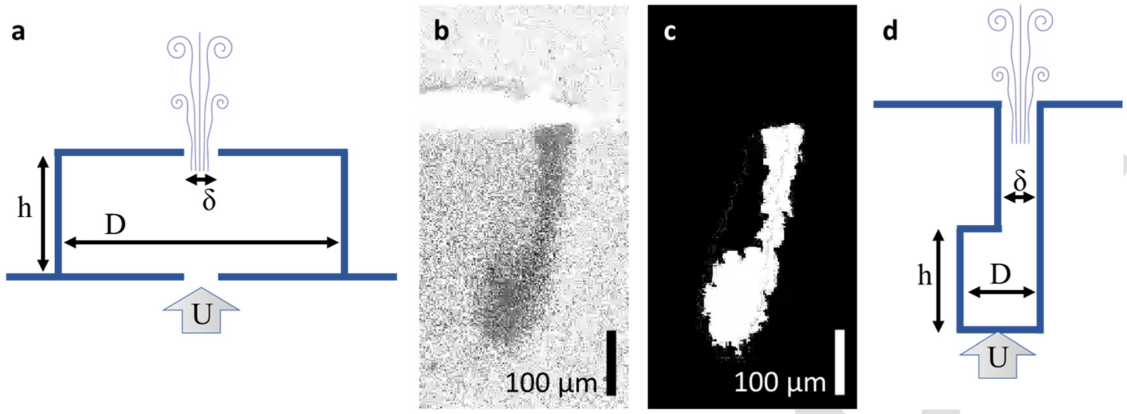

FIG. 2. (a) Schematic representation of a steam kettle whistle recreated from Ref. 25 with the parameters for air velocity U, whistle diameter D, whistle height h, and opening diameter d. (b) X-ray radiograph of a vapor depression from a laser powder bed fusion scan at 500 mm/s and 300 W. (c) X-ray radiograph of the vapor depression after binarization. (d) Schematic representation of the vapor depression with the same parameters as defined for the steam kettle whistle.

constant Strouhal number behavior across increasing Reynolds number—which indicates class III whistle behavior—will appear as constant Strouhal number behavior across increasing reduced normalized enthalpy.

The Strouhal calculation for our vapor depression system requires evaluation of the opening diameter, gas velocity, and tone frequency. The stochasticity of the melt pool and the associated vapor depression dynamics, especially at higher energy densities, requires approximations to complete these calculations. Our Strouhal number analysis is not sensitive to absolute values, rather the relation between gas velocity, frequency, and opening diameter, and how each scales with normalized enthalpy. For gas velocity U, we point to a study that used a Knudsen layer approach to show that gas velocity normal to the powder bed surface scales linearly with normalized enthalpy for stainless steel over ranges of 300–1200 m/s and 50–200 W for scan speed and laser power, respectively.[47] The present work operates within the same regime of normalized enthalpy when accounting for material and thermal properties as well as processing conditions. As such, we proceed in our Strouhal number analysis with gas velocity scaling linearly with reduced normalized enthalpy from 0.3 to 1.5 km/s over the range explored.

The tone frequency and opening diameter are observed to fluctuate within a single track at higher normalized enthalpies, specifically in the unstable keyhole regimes where the vapor depression itself is known to dramatically fluctuate. Assigning a single value to tone frequency or opening diameter for a given track would be misleading given the fluctuations. To address this, we look at the time dependence of tone frequency and vapor depression geometry to assign an upper and lower bound for both frequency and opening diameter for each given track, with smaller opening diameter corresponding to higher frequency and larger with lower. As such, two Strouhal numbers will be calculated for each given track. Opening diameter, d, is measured from binarized in situ x-ray imaging data. For each image frame captured during the print, the minimum width of the vapor depression is identified, and, for each track, these minimum widths are used to determine an upper and lower bound for opening diameter for the track.

Figure 3 shows the plot of Strouhal number vs reduced normalized enthalpy with delineations made to illustrate the conduction, stable keyhole, and unstable keyhole regimes. The conduction and keyhole regimes are differentiated by the geometric aspect ratio of the vapor depression while the stable and unstable keyhole regimes are differentiated by ex situ pore identification. The acoustic data presented in Fig. 1(a) nominally correspond to the conduction regime and exhibit constant frequency behavior—similar to steam kettle whistles at low Reynolds number.[42] While the stable keyhole regime may act as a transitional regime, the unstable keyhole regime, where substantial frequency fluctuations occur in the acoustic data, exhibits constant Strouhal number behavior. Based on the whistle model, constant Strouhal number behavior observed here at higher laser powers reflects class III whistle acoustics, which corresponds to vortex shedding at the end of a resonating duct. These findings are consistent with recent

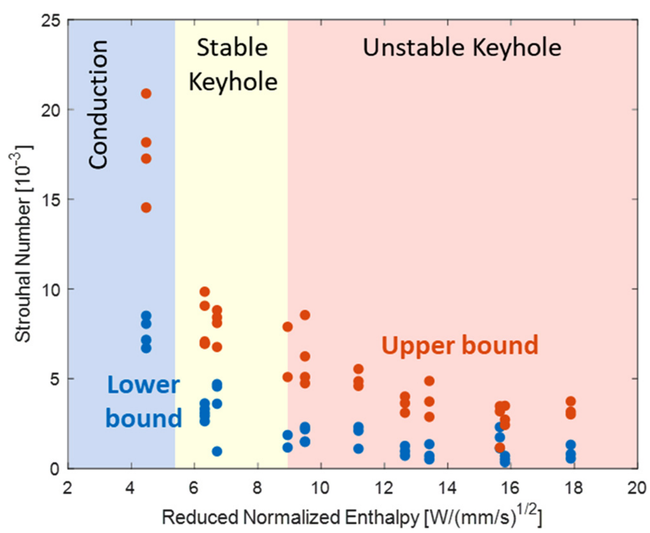

FIG. 3. Plot of the non-dimensionalized Strouhal number as a function of normalized enthalpy for single-track irradiations on Ti-6Al-4V bare plate. Conduction and keyhole regimes are differentiated by the geometric aspect ratio of the vapor depression. Stable and unstable keyhole regimes are differentiated by *ex situ* pore identification.

plume imaging works showing plume structure indicative of vortex shedding at higher laser powers[48] and can be used to better understand and further interpret melt pool morphology.

The present work demonstrates that the aeroacoustic principles present in steam kettles also apply to LPBF melt pools so long as the vapor depression morphology matches the whistle model—i.e., a narrower opening downstream of a larger chamber. This understanding allows a more detailed interpretation of the information-rich acoustic data associated with melt pool behavior in the unstable keyhole regime. For example, Fig. 4 shows the time-dependent acoustic data corresponding to a print at 500 mm/s and 400 W [previously presented in Fig. 1(c)] with binarized images of the vapor depression geometries corresponding to four times during the print. The vapor depression at 1.75 ms exhibits two sequences of a narrow opening downstream of a larger chamber while the vapor depression at 3.05 ms exhibits one such sequence—meeting the geometric requirements of the whistle model. The vapor depressions at 2.50 and 3.30 ms do not meet the requirements because they exhibit constant width and monotonically increasing width, respectively.

Correlation of these geometries and times with the acoustic data shows acoustic signals recorded in the two cases where the whistle model requirements are satisfied and shows an absence of acoustic signals where the requirements are unmet. Additionally, the acoustic peak at 1.75 ms apparently spans >15 kHz in frequency space and 0.2 ms in time. This may be linked to the complex geometry of the vapor depression, which shows two openings with differing diameters. Since this print occurs in the constant Strouhal regime, the opening diameter is inversely related to the frequency of the resulting tone. As such, multiple effective whistles within a single vapor depression would conceivably result in acoustic signals spanning greater frequency ranges and even multi-tone signals. The whistle model provides the foundational framework to mechanistically understand the complex acoustic data commonly found in the stable keyhole regime where many LPBF processes operate.

The present work mechanistically links acoustic generation with melt pool dynamics. While snapshots of vapor depression geometries support the whistle model, capturing vapor depression evolution over time would yield a more complete understanding of the complex

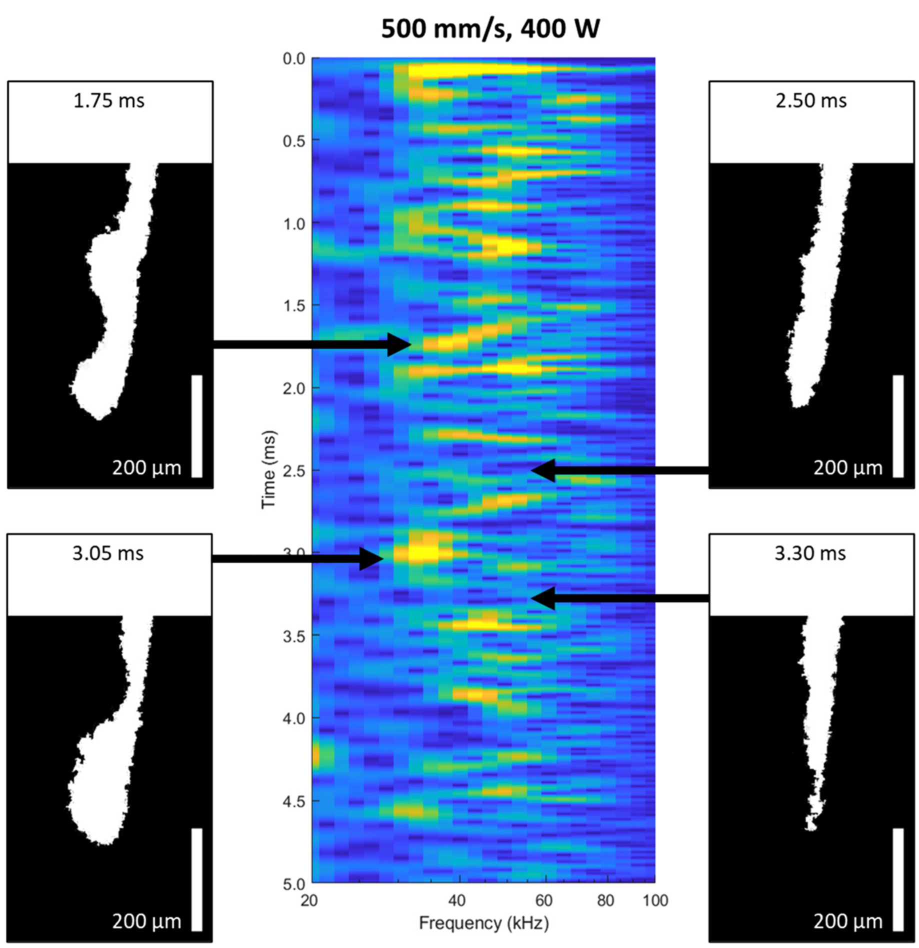

FIG. 4. Time-dependent acoustic data corresponding to a print at 500 mm/s and 400 W previously presented in Fig. 1(c) with binarized images of the vapor depression chosen at four times during the print. The vapor depressions at 1.75 and 3.05 ms (left) fit the geometric requirements of the whistle model whereas the images taken at 2.50 and 3.30 ms (right) do not. Correlation of these times with the time-dependent acoustic data shows acoustic signals at 1.75 and 3.05 ms and shows a lack of signal at 2.50 and 3.30 ms.

acoustic signatures. This is especially true for cases where the acoustic signal appears to persist and shift in frequency over some time—as identified in Fig. 4 and as is characteristic of unstable keyhole behavior. Additionally, extension of this work to better reflect industry-relevant conditions is vital for wider applicability of the present model. This includes powder experiments to investigate the wider validity of the whistle model and full-scale, multi-layer prints to determine the scalability. Further development of the whistle model for vapor depressions will increase the melt pool information extracted from acoustic monitoring and strengthen the overall effectiveness of in situ monitoring techniques.

The whistle model presented offers a direct connection between the acoustic signals captured during the LPBF process and the physical attributes of the melt pool, especially in the keyhole regimes relevant to printing. This model enables interpretation of complex acoustic data to a greater extent than previously available by providing an empirical connection between acoustic frequency and vapor depression geometry via the Strouhal number. The mechanistic understanding of vapor depression aeroacoustics detailed in this work suggests that process monitoring techniques based on acoustic methods will be broadly transferrable to different materials and machine architectures. These findings hope to bridge the gap in physical understanding between acoustic and optical techniques to promote more widespread adoption of acoustic monitoring approaches. By offering insight into the sub-surface morphology of the vapor depression, this model hopes to present acoustic monitoring as a complementary technique to existing optical approaches. With further development of this model, in situ acoustic monitoring can be an accessible and reliable method of probing melt pool dynamics, melt pool depth, and the onset of pore detection in many materials and industrial-scale builds.

Use of the Stanford Synchrotron Radiation Lightsource, SLAC National Accelerator Laboratory, is supported by the U.S. Department of Energy, Office of Science, Office of Basic Energy Sciences (Contract No. DE-AC02-76SF00515). Lawrence Livermore National Laboratory is operated by Lawrence Livermore National Security, LLC, for the U.S. Department of Energy, National Nuclear Security Administration (Contract No. DE-AC52-07NA27344). Some data collection was supported by the LLNL LDRD Program project (No. 21-ERD-008). The LLNL document release number is LLNL-JRNL-857714-DRAFT.

AUTHOR DECLARATIONS

Conflict of Interest

The authors have no conflicts to disclose.

Author Contributions

Yuchen Sun: Conceptualization (lead); Data curation (lead); Formal analysis (lead); Investigation (lead); Validation (lead); Visualization (lead); Writing – original draft (lead); Writing – review & editing (lead). **Sanam Gorgannejad:** Investigation (equal); Methodology (equal); Writing – review & editing (equal). **Aiden Martin:** Investigation (equal); Methodology (equal); Writing – review & editing (equal). **Jenny Nicolino:** Investigation (equal); Methodology (equal). **Maria Strantza:** Investigation (equal); Methodology (equal). **Jean-Baptiste Forien:** Investigation (equal); Methodology (equal). **Vivek Thampy:** Investigation (equal); Methodology (equal). **Sen Liu:** Investigation (equal); Methodology (equal). **Peiyu Quan:** Investigation (equal); Methodology (equal). **Christopher J. Tassone:** Investigation (equal); Methodology (equal). **Manyalibo J. Matthews:** Funding acquisition (equal); Supervision (equal); Writing – review & editing (equal). **Nicholas P. Calta:** Conceptualization (equal); Funding acquisition (lead); Investigation (lead); Methodology (lead); Project administration (lead); Supervision (lead); Writing – review & editing (equal).

DATA AVAILABILITY

The data that support the findings of this study are available from the corresponding author upon reasonable request.

REFERENCES

[1]Wohlers Assoicates, Wohlers Report (Wohlers Assoicates, Fort Collins, CO, 2022).

[2]G. Kasperovich, J. Haubrich, J. Gussone et al., "Correlation between porosity and processing parameters in $TiAl_6V_4$ produced by selective laser melting," Mater. Des. **105**, 160–170 (2016).

[3]S. K. Everton, M. Hirsch, P. Stravroulakis et al., "Review of in-situ process monitoring and in-situ metrology for metal additive manufacturing," Mater. Des. **95**, 431–445 (2016).

[4]A. Ashby, G. Guss, R. K. Ganeriwala et al., "Thermal history and high-speed optical imaging of overhang structures during laser powder bed fusion: A computational and experimental analysis," Addit. Manuf. **53**, 102669 (2022).

[5]C. L. Druzgalski, A. Ashby, G. Guss et al., "Process optimization of complex geometries using feed forward control for laser powder bed fusion additive manufacturing," Addit. Manuf. **34**, 101169 (2020).

[6]S. C. Jensen, J. D. Carroll, P. R. Pathare et al., "Long-term process stability in additive manufacturing," Addit. Manuf. **61**, 103284 (2023).

[7]Z. Y. Chua, I. H. Ahn, and S. K. Moon, "Process monitoring and inspection systems in metal additive manufacturing: Status and applications," Int. J. Precis. Eng. Manuf.-Green. Technol. **4**(2), 235–245 (2017).

[8]T. G. Spears and S. A. Gold, "In-process sensing in selective laser melting (SLM) additive manufacturing," Integr. Mater. Manuf. Innovation **5**(1), 16–40 (2016).

[9]K. Gutknecht, M. Cloots, R. Sommerhuber et al., "Mutual comparison of acoustic, pyrometric and thermographic laser powder bed fusion monitoring," Mater. Des. **210**, 110036 (2021).

[10]F. Imani, A. Gaikwad, M. Montazeri et al., "Process mapping and in-process monitoring of porosity in laser powder bed fusion using layerwise optical imaging," J. Manuf. Sci. Eng. **140**(10), 101009 (2018).

[11]B. Zhang, J. Ziegert, F. Farahi et al., "In situ surface topography of laser powder bed fusion using fringe projection," Addit. Manuf. **12**, 100–107 (2016).

[12]D. Ye, G. S. Hong, Y. Zhang et al., "Defect detection in selective laser melting technology by acoustic signals with deep belief networks," Int. J. Adv. Manuf. Technol. **96**(5–8), 2791–2801 (2018).

[13]S. A. Shevchik, C. Kenel, C. Leinenbach et al., "Acoustic emission for in situ quality monitoring in additive manufacturing using spectral convolutional neural networks," Addit. Manuf. **21**, 598–604 (2018).

[14]Y. Ren, C. Adams, P. Gross et al., "Acoustic data acquisition for quality monitoring during powder bed fusion with laser beam (PBF-LB)," in Daga (■, Hamburg, Germany, 2023). AQ3

[15]J. Petrich, R. W. Smith, and E. W. Reutzel, "Acoustic laser triangulation and tagging for additive manufacturing process monitoring," Int. J. Adv. Manuf. Technol. **129**(7–8), 3233–3245 (2023).

[16]M. Hamidi Nasab, G. Masinelli, C. de Formanoir et al., "Harmonizing sound and light: X-ray imaging unveils acoustic signatures of stochastic inter-regime instabilities during laser melting," Nat. Commun. **14**(1), 8008 (2023).

[17]A. A. Martin, N. P. Calta, S. A. Khairallah et al., "Dynamics of pore formation during laser powder bed fusion additive manufacturing," Nat. Commun. **10**(1), 1987 (2019).

[18]B. Gould, S. Wolff, N. Parab et al., "In situ analysis of laser powder bed fusion using simultaneous high-speed infrared and X-ray imaging," JOM **73**(1), 201–211 (2020).

[19]P. J. DePond, J. C. Fuller, S. A. Khairallah et al., "Laser-metal interaction dynamics during additive manufacturing resolved by detection of thermally-induced electron emission," Commun. Mater. **1**(1), 92 (2020).

[20]M. Seleznev, T. Gustmann, J. M. Friebel et al., "In situ detection of cracks during laser powder bed fusion using acoustic emission monitoring," Addit. Manuf. Lett. **3**, 100099 (2022).

[21]H. Liu, C. Gobert, K. Ferguson et al., "Inference of highly time-resolved melt pool visual characteristics and spatially-dependent lack-of-fusion defects in laser powder bed fusion using acoustic and thermal emission data," Addit. Manuf. **83**, 104057 (2023).

[22]J. R. Tempelman, A. J. Wachtor, E. B. Flynn et al., "Detection of keyhole pore formations in laser powder-bed fusion using acoustic process monitoring measurements," Addit. Manuf. **55**, 102735 (2022).

[23]D. Kouprianoff, I. Yadroitsava, A. du Plessis et al., "Monitoring of laser powder bed fusion by acoustic emission: Investigation of single tracks and layers," Front. Mech. Eng. **7**, 678076 (2021).

[24]D. R. Kouprianoff, "Investigation of acoustic emission signal during laser powder bed fusion at different operating modes," S. Afr. J. Ind. Eng. **32**(3), 279–283 (2021).

[25]K. Xu, J. Lyu, and S. Manoochehri, "In situ process monitoring using acoustic emission and laser scanning techniques based on machine learning models," J. Manuf. Processes **84**, 357–374 (2022).

[26]V. Pandiyan, R. Wrobel, C. Leinenbach et al., "Optimizing in-situ monitoring for laser powder bed fusion process: Deciphering acoustic emission and sensor sensitivity with explainable machine learning," J. Mater. Process. Technol. **321**, 118144 (2023).

[27]H. Wang, B. Li, and F.-Z. Xuan, "Acoustic emission for in situ process monitoring of selective laser melting additive manufacturing based on machine learning and improved variational modal decomposition," Int. J. Adv. Manuf. Technol. **122**(5–6), 2277–2292 (2022).

[28]Z. Li, Z. Zhang, S. Zhang et al., "A novel approach of online monitoring for laser powder bed fusion defects: Air-borne acoustic emission and deep transfer learning," J. Manuf. Processes **102**, 579–592 (2023).

[29]R. Drissi-Daoudi, G. Masinelli, C. de Formanoir et al., "Acoustic emission for the prediction of processing regimes in Laser Powder Bed Fusion, and the generation of processing maps," Addit. Manuf. **67**, 103484 (2023).

[30]Y. Dongsen and Z. Yingjie, "In-situ monitoring of selective laser melting based on heterogeneous integration of acoustic signals and images," in 6th International Conference on Communication, Image and Signal Processing (CCISP) (■, 2021), pp. 420–424.

[31]R. D. Daoudi, "Towards robust monitoring of the laser powder bed fusion process based on acoustic emission combined with machine learning solutions," ■ (Ecole polytechnique federale de Lausanne, 2023). AQ4

[32]S. Gorgannejad, A. A. Martin, J. W. Nicolino et al., "Localized keyhole pore prediction during laser powder bed fusion via multimodal process monitoring and X-ray radiography," Addit. Manuf. **78**, 103810 (2023).

[33]A. A. Martin, J. Wang, P. J. DePond et al., "A laser powder bed fusion system for operando synchrotron x-ray imaging and correlative diagnostic experiments at the Stanford synchrotron radiation lightsource," Rev. Sci. Instrum. **93**(4), 043702 (2022).

[34]C. Zhao, N. D. Parab, X. Li et al., "Critical instability at moving keyhole tip generates porosity in laser melting," Science **370**, 1080–1086 (2020).

[35]L. Guo, H. Wang, H. Liu et al., "Understanding keyhole induced-porosities in laser powder bed fusion of aluminum and elimination strategy," Int. J. Mach. Tools Manuf. **184**, 103977 (2023).

[36]Y. Huang, T. G. Fleming, S. J. Clark et al., "Keyhole fluctuation and pore formation mechanisms during laser powder bed fusion additive manufacturing," Nat. Commun. **13**(1), 1170 (2022).

[37]V. T. Rathod, "A review of acoustic impedance matching techniques for piezoelectric sensors and transducers," Sensors **20**(14), 4051 (2020).

[38]M. Bakhtiari-Nejad, M. R. Hajj, and S. Shahab, "Dynamics of acoustic impedance matching layers in contactless ultrasonic power transfer systems," Smart Mater. Struct. **29**(3), 035037 (2020).

[39]R. C. Chanaud, "Aerodynamic whistles," Sci. Am. **222**(1), 40–48 (1970).

[40]A. Billon, V. Valeau, and A. Sakout, "Two feedback paths for a jet-slot oscillator," J. Fluids Struct. **21**(2), 121–132 (2005).

[41]M.-P. Verge, B. Fabre, A. Hirschberg et al., "Sound production in recorderlike instruments. I. Dimensionless amplitude of the internal acoustic field," J. Acoust. Soc. Am. **101**(5), 2914–2924 (1997).

[42]R. H. Henrywood and A. Agarwal, "The aeroacoustics of a steam kettle," Phys. Fluids **25**(10), 107101 (2013).

[43]S. Ly, A. M. Rubenchik, S. A. Khairallah et al., "Metal vapor micro-jet controls material redistribution in laser powder bed fusion additive manufacturing," Sci. Rep. **7**(1), 4085 (2017).

[44]M. A. Stokes, S. A. Khairallah, A. N. Volkov et al., "Fundamental physics effects of background gas species and pressure on vapor plume structure and spatter entrainment in laser melting," Addit. Manuf. **55**, 102819 (2022).

[45]A. M. Rubenchik, W. E. King, and S. S. Wu, "Scaling laws for the additive manufacturing," J. Mater. Process. Technol. **257**, 234–243 (2018).

[46]M. Naderi, J. Weaver, D. Deisenroth et al., "On the fidelity of the scaling laws for melt pool depth analysis during laser powder bed fusion," Integr. Mater. Manuf. Innovation **12**(1), 11–26 (2022).

[47]P. Bidare, I. Bitharas, R. M. Ward et al., "Fluid and particle dynamics in laser powder bed fusion," Acta Mater. **142**, 107–120 (2018).

[48]I. Bitharas, N. Parab, C. Zhao et al., "The interplay between vapour, liquid, and solid phases in laser powder bed fusion," Nat. Commun. **13**(1), 2959 (2022).